Depletion versus Deflection: How Membrane Bending Can Influence Adhesion

Jin Nam and Maria M. Santore

Department of Polymer Science and Engineering, University of Massachusetts, Amherst, Massachusetts 01003, USA

(Received 2 November 2007; revised manuscript received 15 April 2011; published 9 August 2011)

During depletion-driven vesicle adhesion, a stiff membrane's resistance to bending at fixed tension prevents contact angle equilibrium and vesicle spreading over an opposing vesicle, while more flexible vesicles partially engulf opposing vesicles. Estimates of the bending cost associated with the spreading contact line, relative to the adhesion energy, were consistent with the observed spreading or lack of spreading for the flexible and stiff membranes, respectively, and predicted a lag time sometimes preceding spreading.

DOI: 10.1103/PhysRevLett.107.078101 PACS numbers: 87.16.dm, 62.25.−g, 68.35.Np, 82.35.Gh

Bioadhesion is typically accompanied by membrane deformation: examples include the formation of intercellular adhesion plaques, the action of vesicular delivery packages, and the endocytotic uptake of viruses and nanoparticles. These bioadhesive processes are frequently described in terms of local concentrations of bound and free receptors [1,2]. Membrane mechanics are often neglected since thin cellular membranes are perceived to deform easily. The application of Young's equation to membrane adhesion and engulfment establishes a quantitative analog to droplet spreading or wetting [3–5]. Young's equation relates the contact angle between two adherent giant unilamellar vesicles (in Fig. 1) to the reversible adhesion strength and membrane tension. However, for irreversible adhesion, the advancing contact angle sets the lower bound on the work of adhesion. In other cases, the observed contact angle was smaller than expectations based on the known membrane tension and molecular binding strength [6].

When growth of the contact area between the membrane and a complementary surface requires sharp bending, interfacial mechanics may influence adhesion. This is especially important for synthetic bilayers, stiff capsules, or when a cell membrane is effectively stiffened by association with the underlying actin cortex. Then, the relevant bending modulus κ_b can substantially exceed that of a fluid liposome [7,8], prompting reconsideration of the impact of membrane mechanics on vesicle adhesion and spreading.

Models and simulations anticipate how the energetic costs of membrane bending interfere with membrane adhesion. They predict arrested partial engulfment [9], prevention of spreading [10], instabilities [11], and snapping behavior [11]. Experimentally, a lag time for membrane deformation, followed by sudden spreading (suggestive of instability) has been reported in our [12] and another lab [13]. For instability-related lag times in avidin-biotin-driven membrane adhesion, we formulated a competition between biomolecular adhesive energy and the bending-related line tension, κ_b/r_c, with r_c equal to the radius of curvature of the bent region of the membrane [12]. Uncertainty in the energies and numbers of avidin-biotin bonds confounded a determination of the line tension at the edge of the contact region. The current study quantifies the bending-related line tension by employing depletion-driven binding between vesicle pairs of different flexibility. Large line tensions are revealed, suggesting sharp membrane curvature at the contact line when an adhesive membrane engulfs a target. The study also provides examples of lag-time and snapping behaviors that differ from the phase separation-type instabilities reported for ligand-receptor binding at low membrane tensions [2,13].

This work compares the adhesion of stiff and flexible vesicle pairs subject to depletion forces from dissolved polyethylene glycol (PEG 8 K molecular weight, Polysciences). The expected depletion attractions were calculated from the osmotic pressures of the PEG solutions using a mean-field treatment [4]. "Flexible" vesicles (κ_b = 9.6 + 2.4 kT; thickness = 5 nm [14]) were electroformed from DC5329 from Dow Corning, a 3000 molecular weight graft copolymer with a poly(dimethylsiloxane) backbone and $(EO)_{12}$ (ethylene oxide) side arms, averaging 2 arms

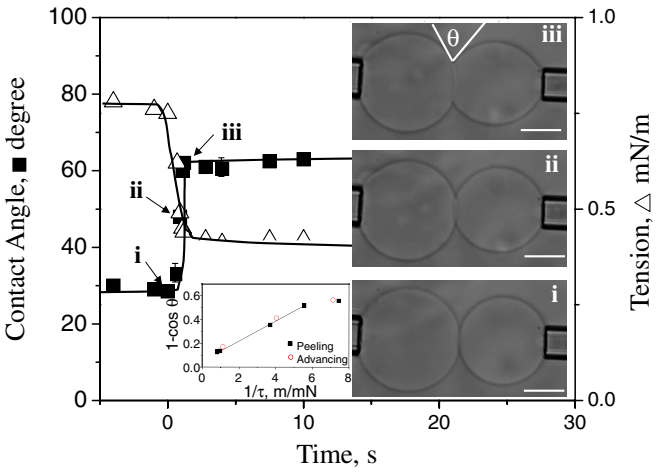

FIG. 1 (color online). Stepwise spreading of flexible vesicles, in 2 wt% PEG solution, with typical error bars. 10 μm scale bars. The inset shows Young's analysis of the work of adhesion.

per molecule. "Stiff" vesicles ($\kappa_b = 26 + 4.5$ kT; thickness = 9.6 nm [8]) were electroformed from a 3800 molecular weight diblock copolymer of poly(butadiene)$_{46}$ and $(EO)_{30}$ from Polymer Labs. Bending moduli were independent of the PEG concentration, in the supporting information.

Dual micropipettes were employed to study vesicle adhesion [1,6,12,15], in the Supplemental Material [16]. One vesicle was held spherical at relatively high tension. The second vesicle at a lower adjustable tension τ between 0 and 1 mN/m, partially engulfed the spherical vesicle. The tension on the second vesicle was reduced and then increased in a stepwise fashion, with equilibration of the contact angle at each tension (waiting about 10 s at each step), and adhesion calculated using a modified Young's equation, $W_a = \tau(1 - \cos\theta)$ [4,5].

Figure 1 illustrates typical depletion-induced adhesion between flexible vesicles in a 2 wt % PEG solution, which produces a calculated attraction of $W_a = 0.03$ mN/m. Upon initial contact (not shown), the low-tensioned vesicle immediately established a "wetted" shape against the spherical vesicle, with sharp membrane bending at the contact line. Then, as the tension of the low tension vesicle was reduced in steps in Fig. 1, the contact area and angle increased quickly. Establishment of the wetted shape was generally observed to be a prerequisite to subsequent increases in the contact area.

Table I summarizes features of depletion-induced adhesion. The inset of Fig. 1 shows an example of Young's equation analysis, with the slope of the graph equal to W_a. Indeed the measured adhesion strengths in Table I were in good agreement with the calculated values, for PEG concentrations of 0.5 wt % and higher, suggesting membrane equilibrium. However, at lower PEG concentrations, 0.1 wt % (for a calculated $W_a = 2.5 \times 10^{-4}$ mN/m), equilibrium spreading, or engulfment was not seen, and the observed contact angles were smaller than predictions from Young's equation.

While flexible vesicles subject to calculated depletion forces exceeding 0.003 mN reached an equilibrated wetted shape, stiff vesicles subject to the same attractive forces did not equilibrate in Table I. For instance, depletion forces of 0.03 mN/m in 2 wt % PEG solution (or more dilute) did not induce spreading, even after ~20 min of contact. Subject to depletion forces of 0.31 mN/m in a 7 wt % PEG solution, stiff vesicles failed to spread for finite membrane tensions, down to 0.01 mN/m: contact angles were smaller than the expected equilibrium values for the known membrane tensions. However, when a slight positive pressure was applied to the right pipette, the right vesicle was made flaccid and gently pushed out of the pipette against the high tensioned vesicle, in Fig. 2. Following a latent time of 80 s from the instant when the suction was decreased to zero, a sharp kink and contact angle were established abruptly (in 0.3 s), followed by spreading at nearly zero membrane tension. The 1–2 min lag time was reproducible for three vesicles tested. Also in Table I, the stronger depletion attractions produced by 10% PEG solutions caused immediate adhesion and spreading of the stiff and flexible vesicles alike.

In Table I, the resistance to adhesive spreading and the lag time seen for the stiff vesicles is similar to previous reports for bioadhesion between lightly functionalized vesicles [12,13]. The current lag time is eliminated by increasing membrane flexibility or depletion forces. Likewise, for avidin-biotin driven adhesion, the lag time was eliminated by increasing the surface density of receptors and ligands [12].

These observations suggest a competition between attractions and membrane bending. Further, the conspicuous sudden snapping of the vesicles into wetted contact, seen with the stiff vesicles in 7 wt % PEG solution [12] suggests an instability. A nucleation-type expression should therefore predict if spreading occurs. Spreading is favored by attractions between vesicles (per unit area) W_a, here from depletion forces, and suppressed by the cost of membrane

TABLE I. Depletion-driven adhesion.

	PEG-8000 concentration	Depletion attraction (calculated)	Spreading kinetics observed	# vesicles	W_a measured	Bending vs binding
Flexible vesicles	10 wt %	0.5 mN/m	Immediate	7	0.65 ± 0.13 mN/m	$\mathbf{E}_{adh} \gg \mathbf{E}_{bend}$
	7 wt %	0.31 mN/m	Immediate	9	0.34 ± 0.07 mN/m	$\mathbf{E}_{adh} \gg \mathbf{E}_{bend}$
	2 wt %	0.03 mN/m	Immediate	9	0.05 ± 0.01 mN/m	$\mathbf{E}_{adh} \gg \mathbf{E}_{bend}$
	0.5 wt %	0.0035 mN/m	Immediate	7	0.009 ± 0.003 mN/m	$\mathbf{E}_{adh} \gg \mathbf{E}_{bend}$
	0.1 wt %	2.5×10^{-4} mN/m	No spreading	6	None	$\mathbf{E}_{adh} \ll \mathbf{E}_{bend}$
Stiff vesicles	10 wt %	0.5 mN/m	Immediate	3	0.62 ± 0.05 mN/m	$\mathbf{E}_{adh} \gg \mathbf{E}_{bend}$
	7 wt % ($\tau \sim 0$)	0.31 mN/m	Time lag then snapping and spreading	3	Snapping prevents measuring advancing angle	$\mathbf{E}_{adh} \approx \mathbf{E}_{bend}$
	2 wt %	0.03 mN/m	No spreading	7	None	$\mathbf{E}_{adh} \ll \mathbf{E}_{bend}$
		$E_{adh} = \pi r_n^2 W_a$			$E_{bend} = 2\pi r_n \kappa_b / r_c$	

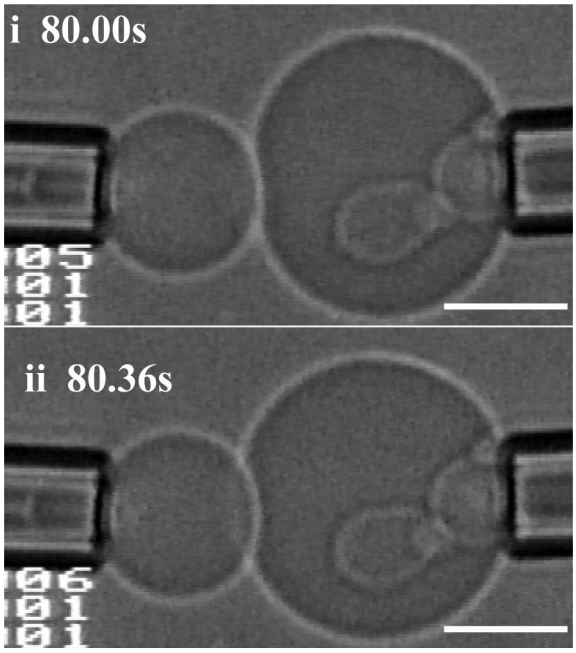

FIG. 2. Stiff vesicles in a 7 wt % PEG solution, with time zero starting when the pressure on the right vesicle became positive. At 80 s, the vesicles snap to form a kink at the perimeter of the contact zone, prior to spreading. The membrane projection, originally in the right pipette, invaginates into the vesicle when the pipette pressure becomes positive. Scale bars are 10 μm.

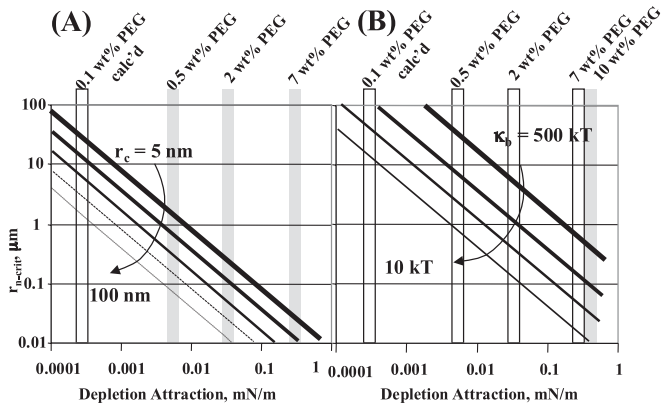

FIG. 3. Radius of critical adhesion nucleus. (a) For flexible membranes with $\kappa_b = 9.6$ kT and variations in r_c: 5, 10, 25, 50, 100 nm; (b) for $r_c = 10$ nm and variations in the membrane stiffness, κ_b: 9.6, 30, 90, and 500 kT. Vertical bars show PEG concentrations corresponding to various depletion forces, with vesicle spreading (gray) and no spreading (white).

bending at the spreading front κ_b/r_c in the form of a line tension. Hence the total energy for an activated spreading process is $E_a = 2\pi r_n \kappa_b/r_c - \pi {r_n}^2 W_a$. Here r_n is the radius of the contact zone, considered a "nucleus."

The spreading or lack of spreading summarized in Table I elucidates the relative bending and adhesive contributions to E_a. The more facile spreading observed for the flexible vesicles suggests a small bending resistance compared with the stiff membranes. With immediate spreading interpreted to indicate $\pi {r_n}^2 W_a \gg 2\pi r_n \kappa_b/r_c$, the appearance of a lag time for a particular PEG concentration (7 wt %) and stiff membranes suggests a similar magnitude of the adhesive attraction and bending resistance. Quantifying the line tension, however, requires consideration of r_n.

The form for E_a suggests that small nuclei are diminished by the cost of bending while above a critical nucleus size, the contact area will grow. The calculated radius of the critical nucleus, $r_{n\text{-crit}} = \kappa_b/(r_c W_a)$, determined by setting first variations in E_a to zero, is shown in Fig. 3. For flexible membranes having $\kappa_b = 9.6$ kT, Fig. 3(a) evaluates several r_c values. For $r_c = 10$ nm, the calculated critical adhesion nuclei are less than 1 μm for the range of polymer concentrations in which spreading was observed. The small $r_{n\text{-crit}}$ values are consistent with the observed spreading because the initial contact between vesicles manipulated via micropipettes is likely about one square micron, circumventing the energy barrier that opposes wetting. (Larger estimates for r_c lower the energy barrier reinforcing this interpretation, and indeed a fixed r_c value need not apply to all polymer concentrations.) Figure 3(a) is consistent with experiments since critical nuclei exceeding a micron are expected for depletion forces of order 0.0001 mN/m [4] (at PEG concentrations of 0.1 wt %) where no spreading was observed.

In Fig. 3(b), if $r_c = 10$ nm, conditions for depletion-driven spreading of the stiff vesicles (with $\kappa_b = 30$ kT) are less favorable in 2 wt % PEG solution ($r_{n\text{-crit}} = 500$ nm) than in Fig. 3(a) for flexible membranes ($r_{n\text{-crit}} = 100$ nm). (Guessing larger values of r_c favors spreading and therefore misses the experimental observations.) One would expect, however, to see even larger critical nuclei for the stiff vesicles, since they spread only when a minimum of 0.5 mN/m attractions are imposed. Hence the observed resistance to spreading for the stiff membranes exceeds the calculated effect. Figure 3(b) includes traces for greater κ_b values to demonstrate the membrane stiffness needed to explain experimental observations, if $r_c = 10$ nm.

If one fixes r_n at a reasonable value for initial contact, then an estimate for the line tension follows from known depletion attractions. For the flexible membranes, Table I indicates $2.5 \times 10^{-4} < E_{\text{bend}}/\pi {r_n}^2 < 0.009$ mN/m, so that for $r_n \sim 1$ μm, $30 < \kappa_b/r_c < 1100$ kT/μm. These seemingly high line tensions are actually moderate (as they allow flexible membrane spreading), and agree with previous order 100 kT/μm estimates [13]. With line tensions in the range 30–1000 kT/μm, the measured value of $\kappa_b = 9.6$ kT suggests the radius of curvature at the contact line is on 10–300 nm. Sharp curvature is consistent with the scaling of r_c as $(\kappa_b/\tau)^{1/2}$ [17]. Since tensions during the spreading of flaccid vesicles approach 1–5 μmN/m and curvatures at the spreading front fall in the range

100–200 nm [17], one expects kink radii as small as 5–10 nm at the contact line when tension is higher, of 0.1–1 mN/m.

For the stiff membranes which resisted spreading at all but the largest PEG concentrations, Table I indicates $0.03 < E_{\mathrm{bend}}/\pi r_n^2 < 0.5$ mN/m and, more specifically at low tensions, that $E_{\mathrm{bend}}/\pi r_n^2 \sim 0.31$ mN/m (75 000 kT/μm^2). Therefore, for $r_n \sim 1$ μm, $3600 < \kappa_b/r_c < 61\,000$ kT/μm, or at lower tensions, 38 000 kT/μm. These line tensions are considerably larger than observed for the flexible membranes. Further setting these values to $(\kappa_b = 30\ \mathrm{kT})/r_c$ leads to $r_c = 8$ nm or less, which is unrealistic.

The explanation lies in the restriction of the classical Helfrich bending treatment to curvatures greater than the membrane thickness [18]. Indeed, experiments reveal increased bending moduli in systems with sharp curvature: as r_c approaches the membrane thickness, κ_b increases sharply and diverges [19]. In the current work, the experimentally measured bending moduli result from the imposition of gentle micron-scale curvature while the local κ_b and r_c during adhesion cannot be measured. The line tension $\kappa_b/r_c \sim 10^3$–10^4 kT/μm^2 is, however, solidly established for the stiff membranes in this study. The observation that the bending line tension is more pronounced than the expected linear dependence in macroscopic κ_b is consistent with the greater thickness of the stiff membranes.

This work demonstrates the influence of the membrane mechanics on adhesion and spreading. Even for modestly stiff membranes, the energetic bending cost can cause a lag time prior to adhesive wetting, produce snapping, or prevent adhesive spreading altogether. This study provides evidence that the curvature associated with spreading can be quite sharp, on the order of 10 nm when the membrane is taut, and this sharpness in curvature may lead to a greater bending cost than would be estimated from macroscopic bending measurements involving radii curvature greater than the membrane thickness. The result is important to an understanding of endocytotic processes and drug delivery by membrane carriers.

This work was made possible by the UMass MRSEC on Polymers, NSF-0932719, NSF-0805061, and the Vanderlick lab at Yale.

[1] D. A. NopplSimson and D. Needham, Biophys. J. **70**, 1391 (1996).
[2] E. Reister-Gottfried *et al.*, Phys. Rev. Lett. **101**, 208103 (2008).
[3] E. A. Evans, Biophys. J. **31**, 425 (1980).
[4] E. Evans and D. Needham, Macromolecules **21**, 1822 (1988).
[5] F. Pincet *et al.*, Biophys. J. **80**, 1354 (2001).
[6] J. J. Lin *et al.*, Langmuir **20**, 5493 (2004).
[7] A. Boulbitch *et al.*, Phys. Rev. E **62**, 3974 (2000).
[8] H. Bermudez, D. A. Hammer, and D. E. Discher, Langmuir **20**, 540 (2004).
[9] K. A. Smith, D. Jasnow, and A. C. Balazs, J. Chem. Phys. **127**, 084703 (2007).
[10] E. Atilgan and B. Ovryn, Biophys. J. **96**, 3555 (2009).
[11] S. Das and Q. Du, Phys. Rev. E **77**, 011907 (2008).
[12] J. Nam and M. M. Santore, Langmuir **23**, 10 650 (2007).
[13] A. Boulbitch, Z. Guttenberg, and E. Sackmann, Biophys. J. **81**, 2743 (2001).
[14] R. M. Hill *et al.*, Langmuir **9**, 2789 (1993).
[15] J. Nam and M. M. Santore, Langmuir **23**, 7216 (2007).
[16] See Supplemental Material at http://link.aps.org/supplemental/10.1103/PhysRevLett.107.078101 for a detailed description of key experimental procedures and measurements of membrane bending moduli.
[17] D. Cuvelier and P. Nassoy, Phys. Rev. Lett. **93**, 228101 (2004).
[18] S. A. Safran, *Statistical Thermodynamics of Surfaces, Interfaces, and Membranes* (Westview Press, Boulder, CO, 2003).
[19] M. Claessens *et al.*, Langmuir **23**, 6315 (2007).